5112 *Chem. Mater.* **2009,** *21,* 5112–5118
DOI:10.1021/cm901928b

CHEMISTRY OF MATERIALS
Article

Nickel Foam Supported-Co_3O_4 Nanowire Arrays for H_2O_2 Electroreduction

Guiling Wang, Dianxue Cao,* Cuilei Yin, Yinyi Gao, Jinling Yin, and Lin Cheng

College of Material Science and Chemical Engineering, Harbin Engineering University, Harbin 150001 P.R. China

Received July 1, 2009. Revised Manuscript Received September 1, 2009

Ni foam supported-Co_3O_4 nanowire arrays are prepared by a template-free growth method, followed by a thermal treatment in air, and are characterized by scanning electron microscopy, transmission electron microscopy, X-ray diffraction, infrared spectroscopy, and thermogravimetric and differential thermal analysis. The Co_3O_4 nanowires have a diameter of about 250 nm, a length up to 15 μm, and a Brunauer-Emmett-Teller surface area of 78.4 $m^2\ g^{-1}$. They grow almost vertically from the surface of Ni foam skeleton, pack densely, and uniformly cover the entire surface of Ni foam skeleton. Electroreduction of H_2O_2 on Co_3O_4 nanowire arrays in alkaline medium is investigated by cyclic voltammetry, chronoamperometry, and electrochemical impedance spectroscopy. The Co_3O_4 nanowire electrode exhibits superior activity, stability, and mass transport property for H_2O_2 electroreduction. A current density of 90 mA cm^{-2} is achieved at −0.4 V in 0.4 mol dm^{-3} H_2O_2 and 3.0 mol dm^{-3} NaOH at room temperature. The per gram current density measured at −0.4 V on Co_3O_4 nanowires is about 1.5 times of that on Co_3O_4 nanoparticles.

Introduction

Fuel cells for use in air-free environments (space and underwater) require liquid or constringent oxygen as oxidant. The bulky tank for carrying oxygen significantly reduces the energy density and safety standard of fuel cell systems. H_2O_2 has been investigated as an alternative oxidant to replace oxygen. Several types of fuel cells using H_2O_2 as oxidant have been reported, such as, direct borohydride−hydrogen peroxide fuel cells[1,2] and metal−hydrogen peroxide semifuel cells.[3−5] Besides its easy handling and storage, H_2O_2 also has faster reduction kinetics than oxygen. The solid/liquid reaction zone at the H_2O_2 cathode is easier to realize and maintain than the solid/liquid/gas region at the oxygen cathode. Therefore, fuel cells with H_2O_2 oxidant tend to have high performance and are more compact. The problem of H_2O_2 as oxidant is its chemical decomposition leading to the formation of O_2, which reduces the utilization efficiency of H_2O_2, causes a two-phase counter current flow within the electrode, and adversely affects reactant diffusions.

Electrodes of nanowire arrays standing on a current-collecting substrate have been successfully prepared by various methods, such as, template-free growth[6,7] and template-directed synthesis using anodic aluminum oxide,[8−11] polymer,[12−21] and virus[22] as template, as well as other methods.[23,24] Owing to the unique structure, this type of electrode usually possesses larger electrochemical

*Corresponding author. E-mail: caodianxue@hrbeu.edu.cn.

(1) Ponce de Leon, C.; Walsh, F. C.; Patrissi, C. J.; Medeiros, M. G.; Bessette, R. R.; Reeve, R. W.; Lakeman, J. B.; Rose, A.; Browning, D. *Electrochem. Commun.* **2008**, *10*, 1610.
(2) Miley, G. H.; Luo, N.; Mather, J.; Burton, R.; Hawkins, G.; Gu, L.; Byrd, E.; Gimlin, R.; Shrestha, P. J.; Benavides, G.; Laystrom, J.; Carroll, D. *J. Power Sources* **2007**, *165*, 509.
(3) Hasvold, O.; Johansen, K. H.; Mollestad, O.; Forseth, S.; Storkersen, N. *J. Power Sources* **1999**, *80*, 254.
(4) Medeiros, M. G.; Bessette, R. R.; Deschenes, C. M.; Patrissi, C. J.; Carreiro, L. G.; Tucker, S. P.; Atwater, D. W. *J. Power Sources* **2004**, *136*, 226.
(5) Yang, W.; Yang, S.; Sun, W.; Sun, G.; Xin, Q. *Electrochim. Acta* **2006**, *52*, 9.
(6) Li, Y.; Tan, B.; Wu, Y. *J. Am. Chem. Soc.* **2006**, *128*, 14258.
(7) Li, Y.; Tan, B.; Wu, Y. *Nano Lett.* **2008**, *8*, 265.
(8) Zhao, G.-Y.; Xu, C.-L.; Guo, D.-J.; Li, H.; Li, H.-L. *J. Power Sources* **2006**, *162*, 492.
(9) Liang, Y.; Zhen, C.; Zou, D.; Xu, D. *J. Am. Chem. Soc.* **2004**, *126*, 16338.
(10) Zhao, N.; Wang, G.; Huang, Y.; Wang, B.; Yao, B.; Wu, Y. *Chem. Mater.* **2008**, *20*, 2612.
(11) Zhang, X. Y.; Zhang, L. D.; Chen, W.; Meng, G. W.; Zheng, M. J.; Zhao, L. X.; Phillipp, F. *Chem. Mater.* **2001**, *13*, 2511.
(12) Patrissi, C. J.; Martin, C. R. *J. Electrochem. Soc.* **2001**, *148*, A1247.
(13) Li, N.; Martin, C. R.; Scrosati, B. *Electrochem. Solid-State Lett.* **2000**, *3*, 316.
(14) Li, N.; Patrissi, C. J.; Che, G.; Martin, C. R. *J. Electrochem. Soc.* **2000**, *147*, 2044.
(15) Nishizawa, M.; Mukai, K.; Kuwabata, S.; Martin, C. R.; Yoneyama, H. *J. Electrochem. Soc.* **1997**, *144*, 1923.
(16) Patrissi, C. J.; Martin, C. R. *J. Electrochem. Soc.* **1999**, *146*, 3176.
(17) Sides, C. R.; Martin, C. R. *Adv. Mater.* **2005**, *17*, 125.
(18) Sides, C. R.; Croce, F.; Young, V. Y.; Martin, C. R.; Scrosati, B. *Electrochem. Solid-State Lett.* **2005**, *8*, A484.
(19) Li, N.; Martin, C. R. *J. Electrochem. Soc.* **2001**, *148*, A164.
(20) Taberna, P. L.; Mitra, S.; Poizot, P.; Simon, P.; Tarascon, J. M. *Nat. Mater.* **2006**, *5*, 567.
(21) Thurn-Albrecht, T.; Schotter, J.; Kastle, G. A.; Emley, N.; Shibauchi, T.; Krusin-Elbaum, L.; Guarini, K.; Black, C. T.; Tuominen, M. T.; Russell, T. P. *Science* **2000**, *290*, 2126.
(22) Nam, K. T.; Kim, D.-W.; Yoo, P. J.; Chiang, C.-Y.; Meethong, N.; Hammond, P. T.; Chiang, Y.-M.; Belcher, A. M. *Science* **2006**, *312*, 885.
(23) Feng, X.; Shankar, K.; Varghese, O. K.; Paulose, M.; Latempa, T. J.; Grimes, C. A. *Nano Lett.* **2008**, *8*, 3781.
(24) Lee, E. P.; Peng, Z.; Cate, D. M.; Yang, H.; Campbell, C. T.; Xia, Y. *J. Am. Chem. Soc.* **2007**, *129*, 10634.

Published on Web 10/07/2009

active surface area, higher utilization efficiency of the active materials, and superior mass transport property than conventional electrodes fabricated by mixing and pressing powder of active material with conducting materials (e.g., carbon black) and polymer binders (e.g., polytetrafluorethylene). Martin and co-workers[12−19] extensively investigated the preparation of nanowire arrays of V_2O_5, SnO_2, $LiMn_2O_4$, and $LiFePO_4$ using a porous polymer membrane template method and found that these nanowire arrays as Li-ion battery electrodes show better rate capabilities than conventional electrodes composed of the same materials. Recently, the research groups of Belcher[22] and Wu[6,7] reported the synthesis of Co_3O_4 nanowire arrays using virus-templated and template-free methods, respectively. These Co_3O_4 nanowires displayed high capacity and rate capability as the anode material for Li-ion batteries. The reversible capacity reached around 700 mAh g^{-1}, which is twice that of current graphite anode. Li and co-workers[8] investigated the performance of Pt and Pt−Ru nanowire array electrodes obtained via an anodic aluminum oxide (AAO) template on a Ti/Si substrate as the anode of direct methanol fuel cell and found that these electrodes have a high electrode area and the surface of the metals is nearly one hundred percent used in contrast to the traditional gas diffusion electrode, in which the utilization of the surface of the catalysts is usually less than 85% due to the addition of carbon and polymer binder. Our recent study demonstrates that Co_3O_4 nanoparticles exhibited promising activity and stability for catalytic electroreduction of H_2O_2 in alkaline medium.[25] The reduction occurs mainly via a direct pathway at low H_2O_2 concentration, e.g., less than 0.5 mol dm^{-3}. However, the Co_3O_4 nanoparticle electrode has to be prepared by a conventional method of mixing Co_3O_4 powder with carbon and polymer binder and pressing the mixture onto a conducting substrate. The resulting electrode usually suffers drawbacks of low active material utilization due to presence of inaccessible regions to the electrolyte solution and poorly controlled porous structure which limited the mass transport of reactants within the electrode.

In this study, cobalt oxide nanowires freely standing on nickel foam were prepared via a template-free growth method. Their morphology, structure, and catalytic activity for H_2O_2 electroreduction in alkaline medium were investigated. Nickel foam served as both the current collector and substrate of nanowires. Its three-dimensional network structure with micro open cages and zigzag flow channels render the electrode with excellent mass transport property and large surface area per unit volume.

Experimental Section

Ni foam supported-cobalt oxide nanowire electrodes were prepared via a template-free growth method.[6,7,26] $Co(NO_3)_2$ (10 mmol) and NH_4NO_3 (5 mmol) were dissolved in a solution consisting of 35 cm^3 H_2O and 15 cm^3 ammonia (30 wt %). The solution, after being magnetically stirred for 10 min in air at room temperature, was transferred to a covered Petri dish and heated in an oven at 90 ± 1 °C for 2 h (ready for nanowire growth). Ni foam substrate (length × width × thickness = 14 × 10 × 1.1 mm, 110 PPI, 320 g m^{-2}; Changsha Lyrun Material Co., Ltd. China) was degreased with acetone, etched with 6.0 mol dm^{-3} HCl for 15 min, rinsed with water, soaked in 0.1 mmol dm^{-3} $NiCl_2$ for 4 h, and then rinsed with water extensively. The left and right edges (2 mm in width) of the Ni foam sheet were wrapped with Teflon tape and folded to 90°, which serves as the spacer for keeping the nickel foam substrate away from the dish bottom. Nanowire growth was carried by immersing the Ni foam in the reaction solution for 12 h at 90 ± 1 °C. After the covered edges were cut off, the obtained electrodes (10 × 10 × 1.1 mm) were thoroughly washed with H_2O, dried at 60 °C for 2 h (referred to as-prepared), and calcined at temperatures between 200 and 400 °C for 2 h in air. In average, 8 mg nanowires were grown on the 1 cm^2 Ni foam, weighed after calcination at 300 °C.

The morphology was examined by a scanning electron microscope (SEM, JEOL JSM-6480) and a transmission electron microscope (TEM, FEI Teccai G2 S-Twin, Philips). The structure was analyzed using an X-ray diffractometer (Rigaku TTR III) with Cu Kα radiation (λ = 0.1514178 nm). Chemical bonding information on metal−oxygen, hydroxyl, and intercalated nitrate anions were investigated with Fourier transform infrared spectroscopy (FTIR, Equinos55, Bruker) using the potassium bromide pellet technique. Each FTIR spectrum was collected after 16 scans with a resolution of 0.5 cm^{-1}. Thermogravimetric and differential thermal analysis (TG/DTA) was performed with a Pyris-Diamond thermal analyzer (Perkin-Elmer) in a flow of air (40 cm^{-3} min^{-1}) at a heating rate of 20 °C min^{-1} from room temperature up to 800 °C in an Al_2O_3 sample pan. Brunauer-Emmett-Teller (BET) surfaces were measured by nitrogen adsorption isotherms recorded on a Micromeritics ASAP 2020 volumetric adsorption system.

Cyclic voltammetric (CV), chronoamperometric, and electrochemical impedance (EIS) experiments were performed in a conventional three-electrode electrochemical cell using a computerized potentiostat (Autolab PGSTAT302, Eco Chemie) controlled by GPES software. Ni foam (1 cm^2 nominal planar area) supported nanowire arrays acted as the working electrode. A glassy carbon rod behind a D-porosity glass frit was employed as the counter electrode to minimize the effect of H_2O_2 decomposition. A saturated Ag/AgCl, KCl electrode served as the reference. All potentials were referred to the reference electrode. All electrochemical measurements were performed at room temperature. The electrolyte was 3.0 mol dm^{-3} aqueous NaOH solution. All solutions were made with analytical grade chemical reagents and Millipore Milli-Q water (18 MΩ cm). EIS measurements were performed by applying an AC voltage with 5 mV amplitude in a frequency range from 0.01 to 100 kHz.

Results and Discussion

Characterization of Cobalt Oxide Nanowire Arrays. Figure 1 shows the SEM images of the electrode calcined at 300 °C. Clearly, the skeletons of Ni foam were completely covered by nanowires, which grow densely and almost vertically from the substrate. The shiny Ni foam substrate turned to black after nanowire growth. The nanowires have diameters of around 250 nm, lengths up

(25) Cao, D.; Chao, J.; Sun, L.; Wang, G. *J. Power Sources* **2008**, *179*, 87.
(26) Marbán, G.; Lópeza, I.; Valdés-Solís, T.; Fuertesa, A. B. *Int. J. Hydrogen Energy* **2008**, *33*, 6687.

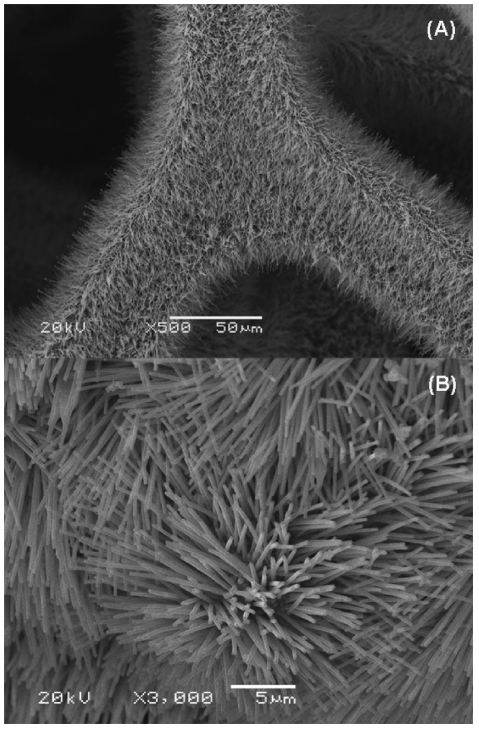

Figure 1. SEM images of nanowires calcined at 300 °C.

to around 15 μm, and fairly good uniformity. The as-prepared electrode demonstrated similar morphology with that calcined, indicating that the nanowire arrays were formed within the growth period in the solution. Figure 2 shows the TEM images of a single nanowire as-prepared (Figure 2A) and calcined at 300 °C (Figure 2B−D). The as-prepared nanowire looks assembled by nanospheres. After calcination, nanospheres break down to nanoparticles with irregular shape and are packed roughly layer by layer to form the nanowires which have a more flat surface (Figure 2B,C). The high resolution TEM (Figure 2D) shows lattice fringes, which combined with the X-ray diffraction (XRD) results below indicate the high-crystalline nature of the building blocks of the nanowires.

Figure 3 shows the XRD patterns of the nanowires. The as-prepared nanowires have the mixed brucite β-$Co(OH)_2$ phase and spinel Co_3O_4 phase, which suggested that partial Co^{2+} was oxidized to Co^{3+} during the period of the reaction solution preparation and the nanowire growth. This is supported by the color change of reaction solution from the original pink to black. The XRD pattern of the nanowires heated at 300 °C in air matches the pattern of pure spinel phase Co_3O_4, showing that $Co(OH)_2$ was converted into Co_3O_4 by the thermal treatment, probably via the reaction between $Co(OH)_2$ and O_2 in air. Peak broadening reflects the nanoplatelet nature of Co_3O_4 building blocks as shown in Figure 2C. It should be pointed out that the presence of α-type cobalt hydroxide in the as-prepared nanowires could not be excluded even though they were not observed in the XRD spectra. The synthesis of α-type cobalt hydroxide using $Co(NO_3)_2$ and ammoniacal solutions under similar

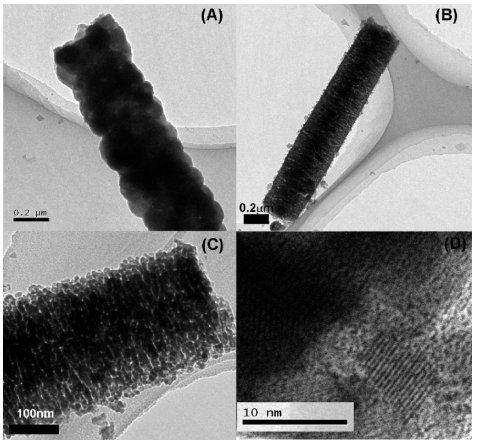

Figure 2. TEM images of a single nanowire: (A) as-prepared and (B−D) calcined at 300 °C.

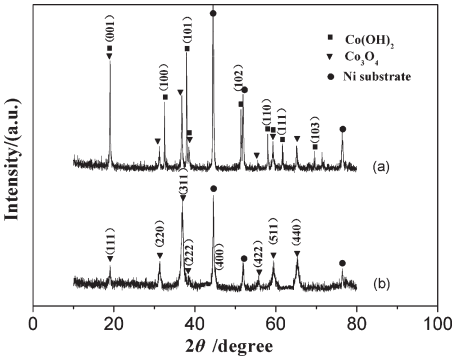

Figure 3. XRD patterns of the nanowires scratched down from Ni foam substrate: (a) as-prepared and (b) calcined at 300 °C.

conditions used in this work has been reported.[27,28] α-Type cobalt hydroxides are layered compounds consisting of positively charged layers with anions and solvent molecules residing in the gallery to restore charge neutrality. They were usually obtained in the form of poorly or turbostratically crystallized aggregates, owing to their metastable feature, and may not be observed in the XRD.[27−32]

The FTIR spectra of the as-prepared and calcined sample are shown in Figure 4. The difference between the two spectra is the presence of two clear peaks at 1384 and 3627 cm^{-1} in the spectrum of the as-prepared nanowires. The weak peak around 1384 cm^{-1} can be attributed to a ν_3 vibrational mode with D_{3h} symmetry of NO_3^-, which possibly is adsorbed in the sample or intercalated in the interlayers of α-type cobalt hydroxide (an indication of the presence of α-type cobalt hydroxides). The strong sharp peak around 3627 cm^{-1} comes from the O−H stretching vibrations of $Co(OH)_2$, which, combining with the XRD analysis (Figure 3), supports the conclusion that the as-prepared sample contains $Co(OH)_2$. The

(27) Xu, Z. P.; Zeng, H. C. *Chem. Mater.* **1999**, *11*, 67.
(28) Rajamathi, M.; Kamath, P. V.; Seshadri, R. *Mater. Res. Bull.* **2000**, *35*, 271.
(29) Xu, R.; Zeng, H. C. *Chem. Mater.* **2003**, *15*, 2040.
(30) Ma, R.; Liu, Z.; Takada, K.; Fukuda, K.; Ebina, Y.; Bando, Y.; Sasaki, T. *Inorg. Chem.* **2006**, *45*, 3964.
(31) Jayashree, R. S.; Kamath, P. V. *J. Mater. Chem.* **1999**, *9*, 961.
(32) Zhu, Y.; Li, H.; Koltypin, Y.; Gedanken, A. *J. Mater. Chem.* **2002**, *12*, 729.

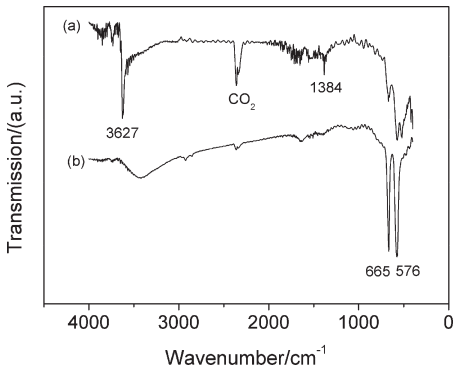

Figure 4. FTIR spectra of the nanowires scratched down from Ni foam substrate: (a) as-prepared and (b) calcined at 300 °C.

absorption bands shown at 665 and 576 cm^{-1} in the spectra of both as-prepared and calcined sample originate from the stretching vibrations of the metal−oxygen bond in the spinel metal oxide, further demonstrating the presence of Co_3O_4 in the as-prepared sample. The broad peak around 3440 cm^{-1} can be assigned to hydrogen bonded O−H stretching of OH in brucite Co(OH) and adsorbed and intercalated H_2O as well. The water bending mode is also found at around 1650 cm^{-1}. All these peaks are well documented in the literature.[27−29,33] The 3627 and 1384 cm^{-1} peaks completely disappeared in the spectrum of the calcined sample, showing that cobalt hydroxides were completely converted to Co_3O_4 after calcination at 300 °C.

Figure 5 represents the TG and DTA curve of the as-prepared sample measured under air flow. The weight loss of the as-prepared sample was clearly observed during the heating process, which takes place roughly in three stages noted by stage I, II, and III on the graph. The weight loss in the range of 23−165 °C (domain I) can be assigned to the evaporation of water physically adsorbed on the surface, trapped in intercrystallite pores, and intercalated in the interlayer space.[28,29,34] Other weakly absorbed species might also contribute to this loss. The domain II ranging from 165 to 220 °C is associated with the loss of water produced by dehydroxylation of the cobalt hydroxides through oxidation with oxygen combined with the loss of parts of nitrate anionic species.[35,36] The domain III ending at about 580 °C can be attributed to the loss of residue nitrate anions and hydroxyl groups.[28] The water content in the as-prepared sample was about 1% estimated from the weight loss in domain I. The total weight loss in domains II and III (165−580 °C) is 12%, which is lower than the theoretical weight loss corresponding to the departure of hydroxyl groups in $Co(OH)_2$ together with the conversion into Co_3O_4 (13.6%). The discrepancy originates from the existence of Co_3O_4 in the as-prepared sample and indicates the very low content of Co_3O_4 in the as-prepared sample.

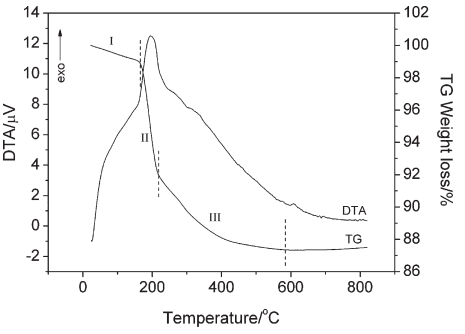

Figure 5. TD/DTA curves of the as-prepared nanowires scratched down from Ni foam substrate.

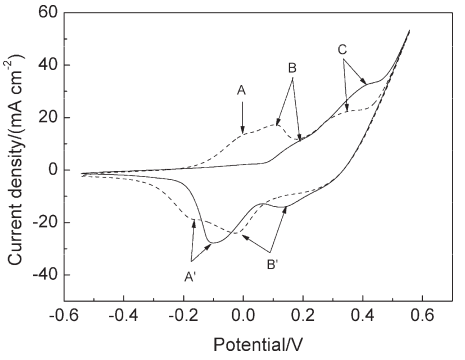

Figure 6. Cyclic voltammograms of the Ni foam supported nanowire electrodes: dash line, as-prepared; solid line, calcined at 300 °C. Electrolyte: 3.0 mol dm^{-3} NaOH. Scan rate: 5 mV s^{-1}.

Catalytic Behavior of Cobalt Oxide Nanowire Array Electrode. Cyclic voltammograms of as-prepared and calcined samples were recorded in NaOH solution at a scan rate of 5 mV s^{-1}(Figure 6). Three (A, B, and C) and two (B and C) anodic peaks were observed on the as-prepared sample and the sample calcined at 300 °C, respectively. These peaks can be attributed to the conversion between different cobalt oxidation states, that is, Peaks A, B, and C correspond to the oxidation of $Co(OH)_2$ to Co_3O_4, Co_3O_4 to $Co(OH)_3$, and $Co(OH)_3$ to CoO_2, respectively.[37−39] Peak A did not occur on the sample calcined at 300 °C, indicating that $Co(OH)_2$ was converted to Co_3O_4 after calcination, which is consistent with the result of XRD (Figure 3) and FTIR analysis (Figure 4). Peaks B and C for Co_3O_4 occurred at more positive potential than that for $Co(OH)_2$. This peak shift likely results from the structure difference of the two compounds. The cathodic peaks can be assigned to the reduction of $Co(OH)_3$ to Co_3O_4 (B′) and Co_3O_4 to $Co(OH)_2$ (A′), respectively. The redox couple of $Co(OH)_2$/Co_3O_4 (A−A′) is likely responsible for the catalytic activity of H_2O_2 reduction because its redox potential is close to the onset potential for H_2O_2 reductions (around −0.1 V; see figure 7).[25]

Figure 7 shows the influence of calcination temperature on catalytic activity for H_2O_2 electroreduction in NaOH

(33) Kandalkar, S. G.; Gunjakar, J. L.; Lokhande, C. D. *Appl. Surf. Sci.* **2008**, *254*, 5540.
(34) Barde, F.; Palacin, M. R.; Beaudoin, B.; Delahaye-Vidal, A.; Tarascon, J. M. *Chem. Mater.* **2004**, *16*, 299.
(35) Poul, L.; Jouini, N.; Fievet, F. *Chem. Mater.* **2000**, *12*, 3123.
(36) Jiu, J.; Ge, Y.; Li, X.; Nie, L. *Mater. Lett.* **2002**, *54*, 260.
(37) Barbero, C.; Planes, G. A.; Miras, M. C. *Electrochem. Commun.* **2001**, *3*, 113.
(38) Hu, C.-C.; Hsu, T.-Y. *Electrochim. Acta* **2008**, *53*, 2386.
(39) Casella, I. G.; Gatta, M. *J. Electroanal. Chem.* **2002**, *534*, 31.

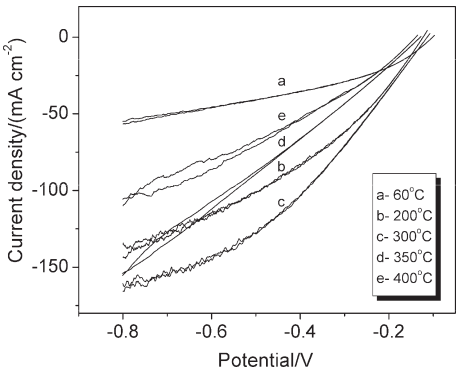

Figure 7. Current−potential polarization curves for H_2O_2 electroreduction on electrodes calcined at various temperatures. Electrolyte: 3.0 mol dm^{-3} NaOH + 0.4 mol dm^{-3} H_2O_2. Scan rate: 5 mV s^{-1}.

Table 1. BET Surface Area of the Nanowires Calcined at Different Temperatures

calcination temperature/°C	60	200	300	350	400
BET surface area/m^2 g^{-1}	76.2	80.3	78.4	26.8	13.5

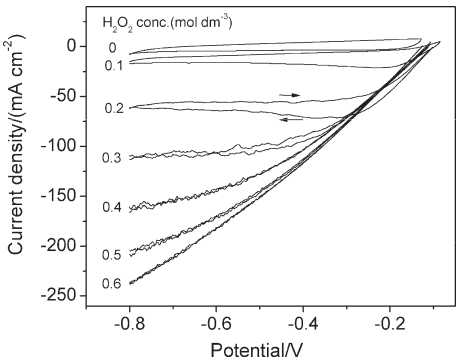

Figure 8. Current−potential polarization curves for H_2O_2 electroreduction at various H_2O_2 concentrations on the electrode calcined at 300 °C. Electrolyte: 3.0 mol dm^{-3} NaOH + H_2O_2. Scan rate: 5 mV s^{-1}.

solution. The polarization curves demonstrate that H_2O_2 electroreduction starts at around −0.1 V and the current density increases with the potential going negatively. The sample calcined at 300 °C (Co_3O_4) exhibits higher activity than that calcined at 200 °C (mixed phase of $Co(OH)_2$ and Co_3O_4) and the as-prepared nanowires ($Co(OH)_2$ in great majority). Since the specific surface area of the samples calcined below 300 °C does not change significantly (Table 1), the activity difference shows that Co_3O_4 has much higher catalytic activity for H_2O_2 electroreduction than $Co(OH)_2$. A further increase in the calcination temperature, higher than 300 °C, results in a decrease in catalytic activity even though the nanowires remain to be Co_3O_4. The loss of activity can be attributed to the decrease of surface area (Table 1), which results from the merge of Co_3O_4 nanowires as clearly shown by the SEM images (Figure 8). Therefore, calcination temperature is critical for obtaining Co_3O_4 nanowires with high surface area.

Figure 9 shows the dependence of the catalytic performance of Co_3O_4 nanowires on the concentration of H_2O_2. The limiting current increased almost linearly with the increase of H_2O_2 concentration below 0.4 mol dm^{-3}. O_2 evolution was observed when H_2O_2 concentration exceeds

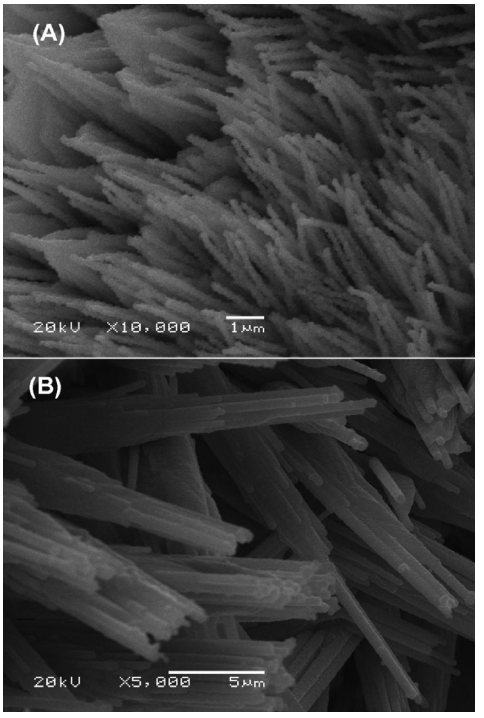

Figure 9. SEM images of nanowires calcined at 350 (A) and 400 °C (B).

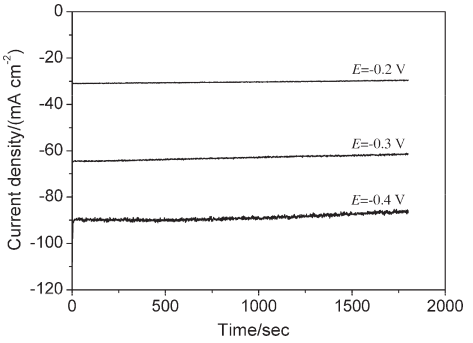

Figure 10. Chronoamperometric curves for H_2O_2 electroreduction on the electrode calcined at 300 °C. Electrolyte: 3.0 mol dm^{-3} NaOH + 0.4 mol dm^{-3} H_2O_2.

0.4 mol dm^{-3}. The onset potential for H_2O_2 electroreduction on Co_3O_4 nanowires is similar to that on Co_3O_4 nanoparticles (around −0.1 V).[25] However, the Ni foam supported-Co_3O_4 nanowire array electrode demonstrated a much lower potential for currents reaching their limits than a Co_3O_4 nanoparticle/carbon/PTFE electrode (e.g., around −0.6 V for nanowire vs −0.35 V for nanoparticles measured in 0.4 mol dm^{-3} H_2O_2 at 5 mV s^{-1}).[25] This suggests that the Co_3O_4 nanowire electrode has much better mass transport performance than the conventional pressed powder electrode.

In order to investigate the stability of the electrode, H_2O_2 electroreduction at various constant potentials was performed. The chronoamperometric curves are shown in Figure 10. Currents remain nearly constant within a 30 min test period, indicating that the Co_3O_4 nanowire electrode has a superior stability for H_2O_2 electroreduction in an alkaline medium. Table 2 lists the mass current density for H_2O_2 electroreduction on a Co_3O_4 nanowire

Table 2. Mass Current Density (mA mg^{-1} Co_3O_4) for H_2O_2 Electroreduction on a Co_3O_4 Nanowire and a Co_3O_4 Nanoparticle Electrode at Different Potentials

potential/V	−0.2	−0.3	−0.4
Co_3O_4 nanowire	0.85	4.0	6.8
Co_3O_4 nanoparticle	3.7	7.6	10.8

(taken from Figure 10) and on a Co_3O_4 nanoparticle electrode (taken from ref 25). The nanowire loading is 8 mg cm^{-2}. The nanoparticles have an average diameter of around 17 nm, and their loading in the electrode is around 15 mg cm^{-2}.[25] Clearly seen from Table 2, Co_3O_4 nanowires show higher steady mass current density than nanoparticles. The current−time curves measured at −0.4 V for the nanowire and nanoparticle electrode also display different features. For the nanoparticle electrode, the currents fluctuate with the increase of time due to the perturbation of oxygen from H_2O_2 decomposition.[25] This negative effect was obviously depressed for the nanowire electrode indicated by the smooth current−time curve. Therefore, the nanowire electrode outperformed the nanoparticle electrode in terms of both activity and mass transport property.

Figure 11 shows the electrochemical impedance spectra of the Co_3O_4 nanowire electrode (the sample calcined at 300 °C) measured at different potentials in NaOH solution with and without H_2O_2. In the absence of H_2O_2, the spectrum displays a semicircle at a high frequency region and a straight line at low frequency region. In the presence of H_2O_2, the spectra at all potentials consist of two slightly depressed semicircles, and the one at the high frequency region closely resembles the one without H_2O_2 and is nearly independent of the potential. It can be attributed to the response of the transition between $Co(OH)_2/Co_3O_4$.[40] The one at low frequency region obviously relates with H_2O_2 because it appears only in the presence of H_2O_2. The diameter of this semicircle becomes smaller when the potential becomes more negative, which suggests that this semicircle most likely corresponds to the electroreduction of H_2O_2 because the reduction rate depends upon the electrode potential, and the lower the potential, the faster the reaction (Figure 10) and the smaller the diameter of the semicircle (Figure 11).[40] The experimental data are simulated by an electrical equivalent circuit composed of two constant phase elements (CPE)/resistive elements in series (inset of Figure 11). The fitting results show that a good agreement between the experimental (symbols) and simulated (solid lines) data was obtained. The fitting parameters of the circuit elements are given in Table 3.

R is the ohmic resistance of the electrolyte and electrode. R_1 and R_2 are the charge transfer resistance of the redox reduction of $Co(OH)_2/Co_3O_4$ and H_2O_2 reduction, respectively. Q_1 and Q_2 are the corresponding constant phase angle elements. Its impedance is defined as $Z_{CPE} = 1/(Q(j\omega)^n)$, in which Q represents the frequency independent parameter, ω is the radial frequency, and n has values $-1 \le n \le 1$. If $n = -1$, CPE behaves as an inductor; if $n = 0$, the CPE behaves as a pure resistor, and if $n = 1$, CPE behaves as a pure capacitor.[41] As can be seen from Table 2, R_1 is around 0.57 Ω cm^2 and is independent of the potential. n_1 is between 0.6 and 0.8, indicating the deviation of Q_1 from the ideal behavior of a perfect capacitor, which might result from the roughness and porosity of the nanowire electrode. R_2 decreases with the potential becoming more negative, showing the H_2O_2 reduction is faster at a more negative potential, which is in good agreement with the results shown in Figure 10. When $n_2 = 1$ (−0.2 to −0.4 V), it implies Q_2 behaves like a capacitor. The two semicircle features in the EIS further suggest that the redox couple of $Co(OH)_2/Co_3O_4$ might be responsible for the catalytic activity of H_2O_2 electroreduction on the Co_3O_4 nanowire electrode.

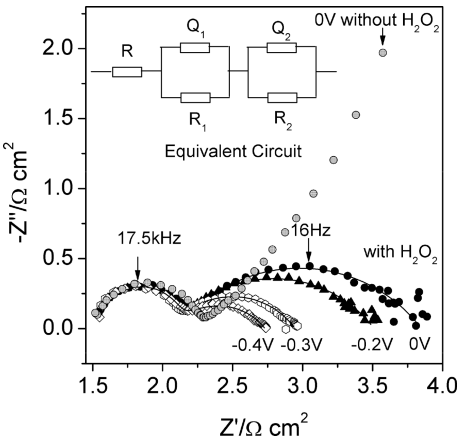

Figure 11. Electrochemical impedance spectra of the nanowire electrode calcined at 300 °C, measured at different bias potentials in the solution of 3.0 mol dm^{-3} NaOH and 3.0 mol dm^{-3} NaOH + 0.4 mol dm^{-3} H_2O_2. Scattered symbols: experimental data points. Solid lines: simulated results. Inset is the equivalent electrical circuit used to fit the experimental data.

Table 3. Values of the Fitting Parameters Evaluated from the Equivalent Circuit at Different Potentials

E/V	R/Ω cm^2	R_1/Ω cm^2	Q_1/mS cm^{-2} s^n	n_1	R_2/Ω cm^2	Q_2/ mS cm^{-2} s^n	n_2
0	1.53	0.58	34.36	0.8	1.74	1.574	0.8
−0.2	1.52	0.57	36.82	0.6	1.43	1.599	1
−0.3	1.51	0.56	32.97	0.6	0.88	0.017	1
−0.4	1.54	0.56	32.16	0.8	0.62	0.018	1

Conclusions

Growth of spinel Co_3O_4 nanowire arrays on Ni foam was successfully demonstrated. The nanowires have diameters of around 250 nm and lengths up to around 15 μm. They densely and vertically stand on the frame of a Ni foam substrate to give a Co_3O_4 nanowire loading of 0.8 mg cm^{-2}. The thermal treatment temperature is very important for the formation of the active Co_3O_4 phase and for the retainment of high active surface area of the electrode. The resulting electrode shows better performance for H_2O_2 electroreduction in an alkaline medium in terms of both activity and mass transport property than a Co_3O_4 nanoparticle/carbon/PTFE electrode. The

(40) Palmas, S.; Ferrara, F.; Vacca, A.; Mascia, M.; Polcaro, A. M. *Electrochim. Acta* **2007**, *53*, 400.

(41) Jorcin, J.-B.; Orazem, M. E.; Pebere, N.; Tribollet, B. *Electrochim. Acta* **2006**, *51*, 1473.

redox couple of $Co(OH)_2/Co_3O_4$ might play an important role in the electrocatalytic reduction of H_2O_2 on the Co_3O_4 nanowire electrode.

Acknowledgment. We gratefully acknowledge the financial support of this research by National Nature Science Foundation of China (20973048), Heilongjiang Provincial Natural Science Foundation (ZJG2007-06-02), Heilongjiang Postdoc Foundation (LBH-Q06091), Key Laboratory of Superlight Materials and Surface Technology of Ministry of Education, and Harbin Engineering University (HEUFT07030, HEUFT07051, and HEUFT08008).